Development of an Innovative 2-DOF Continuous–Rotatable Mechanism

Chun Liu(✉), Ting-Hao Wang, and Pei-Chun Lin(✉)

National Taiwan University, Taipei City 10617, Taiwan (R.O.C.)
{d05522022, wtyngh, peichunlin}@ntu.edu.tw

Abstract. We report on the development of an innovative two degrees of freedoms (DOF) mechanism that is capable of performing continuous rotation in both DOFs. The design process began with the analysis and comparison of general 2-DOF mechanisms with various morphologies. The final selection was based on joint angles that yielded the largest region of continuous rotation. The design concept was realized as an empirical mechanism design. The transmission systems of the two DOFs were carefully designed so that the two DOFs can rotate continuously without colliding with one another. More specifically, double C-shaped racks were designed and utilized as key components to fulfill this goal. The dynamics of the 2-DOF mechanism was then analyzed to better understand the relation between the torque input and the rotation motion output. A prototype was built and its performance was empirically evaluated. The experimental results confirm the functionality of the continuous rotation of the two DOFs in the mechanism.

Keywords: 2-DOF · Mechanism design · Continuous rotation · Joint

1 Introduction

Animals usually have delicate, compact, and efficient joint systems, such as the waist or hip joint, which generate dexterous multi-degrees of freedom (DOF) motion. In contrast, artificial robotic motion systems have thus far mainly relied on one-DOF motors. Therefore, generating multi-DOF motions that mimic wrist or hip joints rely on mechanism designs that couple multiple individual motor motions in a compact form. The wrist joint, for example, is composed of two revolute chains (RR configuration) or a universal joint (U configuration) whose axes of rotation intersect perpendicularly [1]. The empirical two DOFs system driven by motors can be considered as joined by a linkage, and the connection method further determines the range of the joint workspace. Therefore, the connection method should be skillfully designed and optimized to meet the requirements of specific tasks.

2-DOF joints are popular and prevalent in humanoid robots owing to their biomimetic morphology with respect to the human body—for example, the wrists of WABIAN-2 [2] and ARMAR-3 [3], and the ankles of NAO [4], DLR-Biped [5] and LOLA [6]. Different humanoid robots use different linkage connection designs. The WABIAN-2 and ARMAR-3 mimic the motion behaviors of the human wrist favorably. Their design shifts the axis of rotation for intersecting the other axes, and they have

C.-H. Kuo et al. (Eds.): ISRM 2019, MMS 78, pp. 125–137, 2020.
https://doi.org/10.1007/978-3-030-30036-4_11

four support linkages around the motor close to the hand. The ankle of NAO has the same construction. The ankles of DLR-Biped and LOLA have one linkage connecting the motor that drives the foot from the motor near the knee, and they have double support linkages on the feet. In addition, the wrist of ARMAR-4 [7] has three DOFs, and after excluding the first revolute joint, which represents the pronation/supination generated from the forearm [8], the other two can form a 2-DOF structure. The motor that rotates the hand is supported by the C shell from both sides, and only one linkage is connected to the hand. This configuration successfully decreases the structural limitation regarding pitch motion. The three-DOF hip mechanism on HRP-3 [9] and ARMAR-4 [10] can similarly be decomposed. Discarding the joint that preforms lateral/medial rotation [11], the joint of HRP-3 has three support linkages—two for fixing the motor and one for acting as the femur. Moreover, the hip of ARMAR-4 has only two short support linkages to enlarge the rotation range. Because, so far, most of the 2-DOF mechanisms are for humanoid joints, the motion range of these DOFs is usually limited and does not have the possibility of continuous rotation, thus confining the motion range and motion speed.

Here, we report on an innovative 2-DOF mechanism that is capable of performing continuous 2-DOF rotation using a serial RR chain and a novel driving and connecting mechanism to avoid collision. This mechanism can still of course be utilized as a wrist or other joint, but it has extended performance regarding workspace and motion speed owing to continuous rotation. Moreover, this mechanism can be extended to other applications, such as pan-and-tilt cameras with extended surveillance viewing ranges. The contributions of this research include (i) the classification of the rotation behaviors of existing 2-DOF joints; (ii) the development of innovative mechanisms that provide a unique and new rotation behavior; and (iii) the analysis of mechanism dynamics.

The remainder of this work is organized as follows. Section 2 describes the rotation behavior of existing 2-DOF models and their motion and structural limitations. Section 3 describes the mechanism design of the innovative 2-DOF mechanism, which is followed by an analysis of the mechanism dynamics in Sect. 4. Section 5 shows the practical implementation results, and Sect. 6 concludes the work.

2 Rotation Behavior of Existing 2 DOF Structure

A multi-DOF joint inherently assumes that the rotational axes are not parallel to one another for independent motion. In addition, the rotational axes of the joint are usually set to be mutually orthogonal and to intersect one another (i.e. the morphology is similar to the universal joint). This is because complete driving independence of axes yields an easier computation regarding forward and inverse kinematics and dynamics. Thus, this work focuses on this configuration.

Empirically, to drive the described two DOFs requires a specific mechanism design because the motor and transmission system have non-zero physical sizes. Therefore, from the geometric point of view, the workspace or the rotation behavior of the multi-DOF joint depends on the size of the motors as well as the sizes of the transmission system and associated supporting structure. To simplify the analysis, the overall system can be modeled as two cylindrical blocks (M1 and M2) and two linkages (L_1 and L_2).

The cylindrical blocks represent the spaces taken by the motors. The first linkage L_1 represents the transmission system and supporting structure, which transmits the rotational motion of the first motor to the place where the second motor resides so that the two DOFs are mutually orthogonal and intersect one another. The second linkage L_2 represents the end effector. It should be noted that L_1 here is used to transmit the rotation motion but not driven by the motor-1 directly.

Because the motor size (i.e. M1 and M2) is usually fixed and the mechanism design mainly addresses how the motor power transmits to drive the 2-DOF end effector, the following analysis focuses on the variation of the transmission and structure design (i.e. L_1) as well as how the motion can be output to the end effector (i.e. L_2). The mechanism can be classified into four types, which are based on use of single (S) or double (D) connection linkages: DD, DS, SD, and SS. The first letter D/S associated with linkage L_1 represents the use of either one or two sides of spaces between the first DOF (M1) and the second DOF (M2) in the transmission system and structure. The second letter D/S associated with linkage L_2 represents the use of either one or two sides of spaces between the M2 and the end effector by the structure.

The motor size and connection linkage lengths were set, as shown in Table 1, so that comparison among the four types of mechanism (DD, DS, SD, and SS) could proceed. Because blocks M1 and M2 occupy physical space, the linkage L_1 has a minimum length so that the blocks are physically separated in various locations without collision or interference. Similarly, the linkage L_2 has a minimum length so that the output can be transferred to the end effector "outside" the joint for practical uses, such as mounting a camera. The linkage thickness is set to zero but is still present.

Table 1. Geometrical parameters of the modeled 2-DOF joint

Parameter	Unit
Motor radius	8
Motor thickness	6
Linkage length, L_1	4 + 5
Linkage length, L_2	10
Width of linkage	0

Table 2. The D-H parameter of the modeled 2-DOF joint

i	α_{i-1}	a_{i-1}	d_i	θ_i
1	0	0	0	θ_1
2	90	0	0	θ_2

The geometrical relation of the described 2-DOF mechanism can be represented using Denavit–Hartenberg (D–H) notation [12]. Since the four types of mechanism have the same morphology but vary regarding the use of single or double connection methods, the D–H parameters of the four types are identical, as shown in Table 2. Figure 1(a) shows the associated coordinate systems, where the origin is set at the center of M2. The motion ranges of motor-1 and motor-2 are denoted as θ_1 and θ_2, respectively. The first DOF generated by motor-1 rotates around the axis Z_1, and the second DOF generated by motor-2 rotates about axis Z_2. The motion ranges of motor-1 and motor-2 are denoted as θ_1 and θ_2, respectively. Thus, the origin end point of linkages L_2, where θ_1 and θ_2 are 0°, is at $(10, 0, 0)$ for global coordinate. When θ_i is positive number means it rotates anticlockwise around its own Z_i-axis (orange arrows). Conversely, When θ_i is negative number means it rotates clockwise about its own Z_i-axis. With these definitions and settings, the analysis of the 2-DOF joint using the four types can proceed, emphasizing their ability to rotate continuously.

(i) DD: There are four linkages around M2, and the model is shown in Fig. 1(b). The achievable ranges of θ_1 and θ_2 are only $\pm 153.6°$ and $\pm 90°$, respectively, owing to the volumes taken by blocks as well as the double-supported configurations; continuous rotation is therefore not possible with DD.

(ii) DS: The transmission uses spaces on both sides of M1, and the end effector only uses space on one side. The ranges of θ_1 and θ_2 are same as those of DD, but θ_2 can rotate continuously when θ_1 is between $+26.4°$ and $+153.6°$. Figure 1(c) shows the continuous rotation ability of θ_2 by drawing the reachable positions of the end effector (i.e. the green region). The brown curve shows one special condition when θ_2 is 0°.

(iii) SD: The transmission only uses space on one side of M1, and the end effector uses space on both sides, opposite to the DS. The range of θ_1 remains $\pm 153.6°$, and the range of θ_2 is $-149°$ to 90°. Additionally, θ_1 can rotate continuously when θ_2 is within the range $-149°$ to $-31°$. Nevertheless, θ_2 does not have the ability to rotate repetitively due to the double support linkages. Therefore, there is no green region, as shown in Fig.1(d), but the cyan region indicates the ability of θ_1 to continuously rotate, and the brown curve is plotted while θ_1 is 0°.

(iv) SS: Both the transmission and the end effector use space on only one side of M1. The structure of the 2-DOF joint in this configuration has fewer geometric constraints than the other three cases. Although the range of θ_1 is still $\pm 156°$, and the range of θ_2 is between $-149°$ and 90°, θ_1 can rotate continuously when θ_2 is between $-149°$ and $-31°$; θ_2 can also rotate continuously when θ_1 is between 26.4° and 153.6°. Therefore the green area and the cyan area overlap, as shown in Fig. 1(e).

The proposed mechanism design in this work can be classified as type SS, although the arrangement of the transmission and supporting structure (i.e. L_1) differs from the existing SS structure, as the linkage is shifted into the center region between the M1 and M2 blocks. Hereafter, this configuration is referred to as SSD. In this case, L_1 does not interfere with the rotation of θ_2. Therefore, although the rotation range of θ_1 is still restricted to $\pm 153.6°$, the range of θ_2 can be extended on both sides to $\pm 149°$. Moreover, the continuous rotation range for θ_1 is available when θ_2 is between $-149°$ and $-31°$, and between 31° and 149°. Conversely, the continuous rotation range for θ_2 is available when θ_1 is between $-153.6°$ and $-26.4°$, and between 26.4° and 153.6°. As long as θ_1 and θ_2 are within the described range, which is twice that of SS, both DOFs of the SSD can perform continuous rotations simultaneously, as shown in Table 3. The covered region is plotted in Fig. 1(f).

In summary, block M1 affects θ_1 equally for all four types. The linkages L_1 determines the range and continuous rotation ability of θ_1, and the linkage L_2 determines the other DOF, θ_2. Type SS is the only configuration where both θ_1 and θ_2 have the opportunity to perform continuous rotation simultaneously, as shown in Table 3.

In addition, the proposed type SSD doubles the range for continuous rotation and extends the rotation range of θ_2.

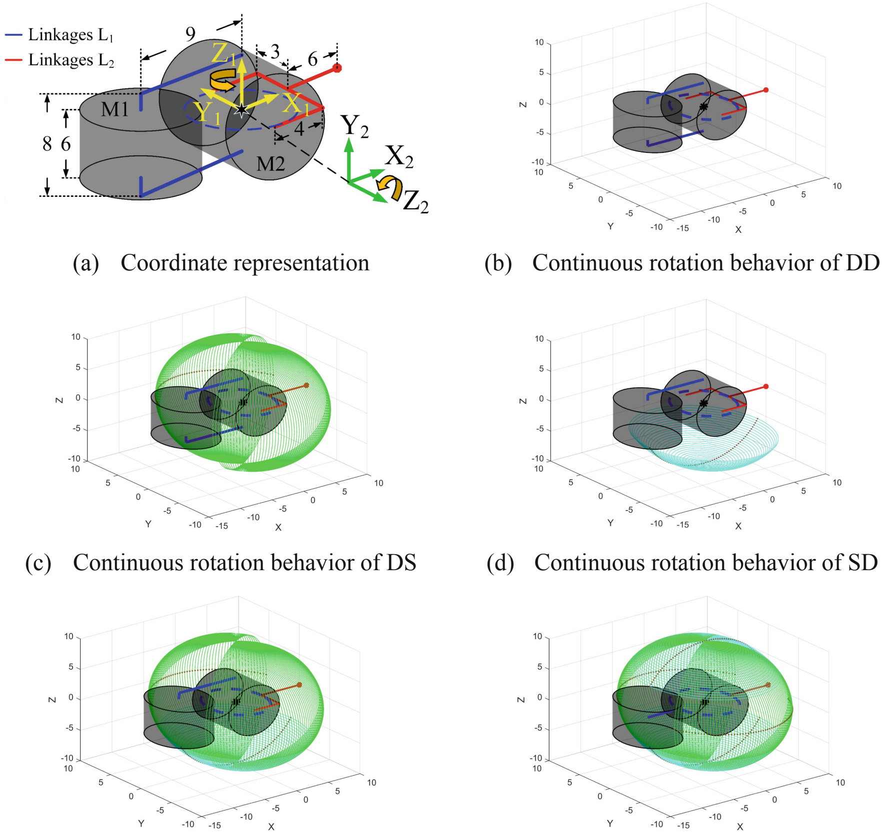

(a) Coordinate representation (b) Continuous rotation behavior of DD

(c) Continuous rotation behavior of DS (d) Continuous rotation behavior of SD

(e) Continuous rotation behavior of SS (f) Continuous rotation behavior of SSD

Fig. 1. Coordinate representation (a), continuous rotation behavior of four stand types (b) DD (c) DS (d) SD (e) SS and the proposed type (f) SSD

Table 3. Rotation range of the DOFs in five different types

	DD	DS	SD	SS	SS design
θ_1	±153.6°	±153.6°	±153.6°	±153.6°	±153.6°
θ_2	±90°	±90°	−149° +90°	−149° +90°	−149° +149°
θ_1 range for θ_2 RC	None	+26.4° +153.6°	None	+26.4° +153.6°	−153.6° ~ −26.4° +26.4° ~ +153.6°
θ_2 range for θ_1 RC	None	None	−149° −31°	−149° −31°	−149° ~ −31° +31° ~ +149°

Note. θ_1 range for θ_2 RC: θ_2 rotate continuously (RC) when θ_1 within the range. θ_2 range for θ_1 RC: θ_1 rotate continuously (RC) when θ_2 within the range.

3 Design and Implementation of the 2-DOF Mechanism

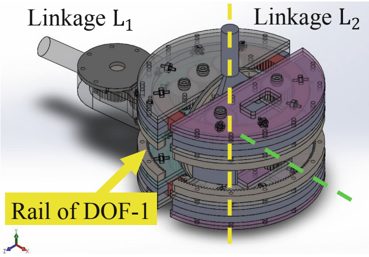

(a) The CAD drawing of the 2-DOf mechanism

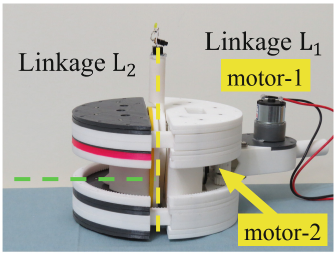

(b) The prototype of the 2-DOF mechanism

Fig. 2. The CAD drawing and the prototype of the 2-DOF mechanism

The mechanism design aims to realize the proposed SSD type, and Fig. 2(a) and (b) show the CAD design and the empirical implementation of the 2-DOF joint, respectively. The final cylinder has a diameter of 180 mm, a thickness of 108 mm, and weighs approximately 2.3 kg. The first DOF, which rotates around yellow axis, is designed to have continuous output rotation, so, conceptually, the output should have a cylindrical shape when the DOF is driven from the motor-1 outside. Motor-1 here is correlated with block M1 in Sect. 2, and by fixing Linkage L_1, the cylinder can rotate along the Rail of DOF-1. In the meantime, to allow the second linkage L_2 located at the center of the cylinder to rotate continuously about green axis without colliding with the cylinder, the cylinder should be divided into two halves; these two halves should be designed to have a specific structure so that the relative configuration can be maintained. To satisfy these two constraints, two rotatable C-shaped structures are utilized to bridge the two halves. When the linkage L_2 rotates and passes the rack, the rack synchronously rotates to the orientation where the gap is presented. In the meantime, the other rack still connects the two cylindrical halves to fix the cylinder structure. This innovative double-C design allows the 2-DOF mechanism to have a wide range of continuous rotations.

Figure 3 demonstrates how the double-C works in detail. The gaps of the two C-shaped racks placed on opposite sides are shown in Fig. 3(a). When the linkage L2 drives the end effector close to the upper C rack, it rotates to the orientation where the gap is presented, as shown in Fig. 3(b). Likewise, when it approaches the lower C rack, as shown in Fig. 3(c), the gap is also presented. In the second half of the rotation (i.e. the linkage is rotated up from the bottom, as shown in Fig. 3(d), a similar process is repeated, as shown in Fig. 3(e) and (f).

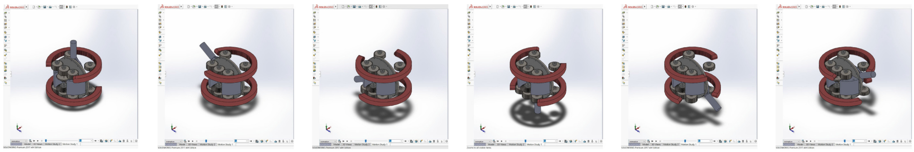

(a) (b) (c) (d) (e) (f)

Fig. 3. Illustrative motion sequence of the 2-DOF mechanism while the second DOF performs continuous rotation

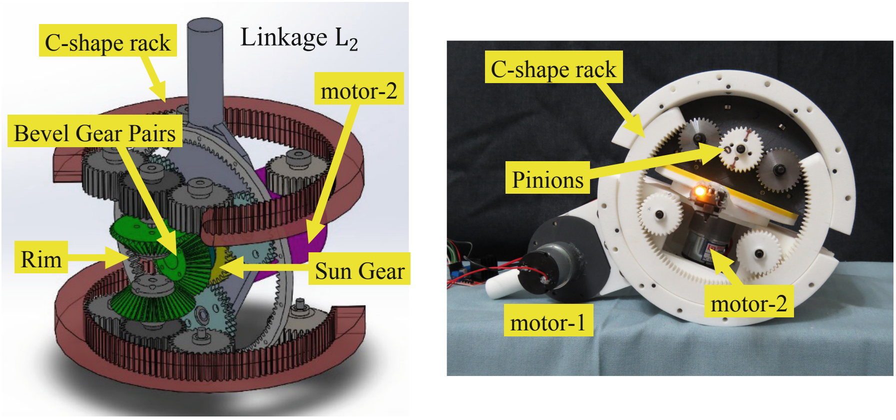

(a) Bevel Gear Pairs and Sun Gear (b) Pinions

Fig. 4. Transmission system of the 2-DOF mechanism

The double-C mechanism described above requires a specific transmission system design. The C racks should be rotated synchronously as motor-2 is driven (i.e. θ_2). In the empirical design, the output of motor-2, which is aligned with block M2 in Sect. 2, drives the linkage L_2, where the linkage is also the arm of the plenary gear system. The rim is structurally fixed to one of the half-cylinders (i.e. does not rotate), and the output is the sun gear. The sun gear transmits the motion to the rack through bevel gear pairs Fig. 4(a) and the pinions Fig. 4(b). As for the first DOF, motor-1 is placed outside the cylinder. Eventually, all the gears driven by linkage L_2 inside utilizes the double-C mechanism, and further realize the behavior of SSD.

4 Dynamic Simulation

Constructing a physical model of the mechanism is necessary to better understand the system dynamics and is helpful during the design and analysis process. In this section, the equation of motion was derived based on the known geometry and mass distribution. Given the initial postures and the rotating trajectories, the required torques to drive the system can be predicted as the reference on selecting the appropriate actuators. Meanwhile, the kinematic can also be acquired with the given driving torque. Through the simulations and visualizations, several control strategies and the corresponding reactions of the system can be supervised before implementing the real mechanism.

To construct the governing equation, we first define the coordinate system. The 2-DOF RR joint can be simplified to two links, denoted as Link 1 and Link 2, and the ground link is denoted as Link 0. The coordinates corresponding to each link, shown in Fig. 5, are set to be concentric, while the z-axis is aligned with the rotating shaft according to the D–H notation. Here, we simply set the center of mass (CoM) to be located along the x-axis, so the representation can be written as ${}^{i}P_{C_i} = L_{C_i}\widehat{x}_i$, where the L_{C_i} is the distance between the CoM and the origin. The rotation of the link is denoted as θ_i, and the mass and inertia tensor of the mechanism are denoted as m_i and I_i, where $i = 1, 2$.

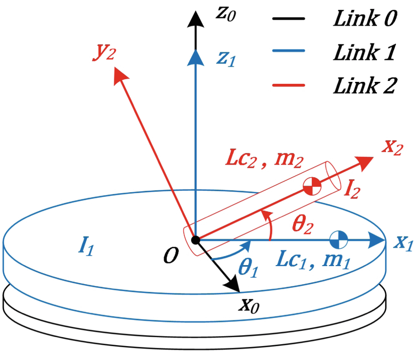

Fig. 5. The model for dynamics analysis

By using either the Newton–Euler approach or the Lagrangian formulation [12], the equation of motion can be obtained with the following formation, which includes mass, centrifugal and Coriolis, gravity, and friction terms:

$$\tau = M(\Theta)\ddot{\Theta} + V\left(\Theta, \dot{\Theta}\right) + G(\Theta) + F\left(\Theta, \dot{\Theta}\right) \tag{1}$$

$$M(\Theta) = \begin{bmatrix} m_1 L_{C_1}^2 + m_2 L_{C_2}^2 \cos\theta_2 + I_{1,zz} & 0 \\ -I_{2,xy}\sin\theta_2 - I_{2,yz}\cos\theta_2 & m_2 L_{C_2}^2 + I_{2,zz} \end{bmatrix} \tag{2}$$

$$V\left(\Theta, \dot{\Theta}\right) = \begin{bmatrix} \left(-2 m_2 L_{C_2}^2 \sin\theta_2 \cos\theta_2\right)\dot{\theta}_1\dot{\theta}_2 \\ \left(\left(m_2 L_{C_2}^2 - I_{2,xx} + I_{2,yy}\right)\sin\theta_2\cos\theta_2 + I_{2,xy}\left(\cos\theta_2^2 - \sin\theta_2^2\right)\right)\dot{\theta}_1^2 \end{bmatrix} \tag{3}$$

$$G(\Theta) = \begin{bmatrix} 0 \\ m_2 L_{C_2}\cos\theta_2 g \end{bmatrix} \tag{4}$$

$$F\left(\Theta,\dot{\Theta}\right)=\begin{bmatrix}B_1\dot{\theta}_1+C_1sgn\left(\dot{\theta}_1\right)\\ B_2\dot{\theta}_2+C_2sgn\left(\dot{\theta}_2\right)\end{bmatrix} \tag{5}$$

Here, B_i is the viscous friction coefficient, C_i is the Coulomb friction coefficient. B_i and C_i are properly set to be specific small values for the initial trials, and further system identification is needed to refine the parameters for better prediction results.

The above equation gives the expressions for the torque of each actuator as a function of joint position, velocity, and acceleration, which means we can predict the required torque with the given motor trajectory. This also corresponds to the case when we apply position control to manipulate the mechanism. Note that when considering the extra load exerted on Link 2, which would be a common situation in practical use, we can simply adjust the corresponding values of L_{C_2} and m_2 to modify the model.

Figure 6 gives a simple example of the simulation under constant ω trajectory input. Figure 6(a) shows the two given trajectories, with the angular velocity values shown in Fig. 6(c). The endpoint trajectory of link 2 on each timestamp is drawn on Fig. 6(b) to check whether the collision between two links would happen, and the calculated torques are shown in Fig. 6(d). In this case, the set of trajectory would lead to collision when θ_1 and θ_2 both approach 0 or π, and it can be prevented through proper adjustments to the initial posture of both links. As far as the torque is concerned, since no angular acceleration is involved, τ_1 is a constant value due to the friction effect, and the τ_2 appears to oscillate with the motion of Link 2 and is mainly related to the gravity effect.

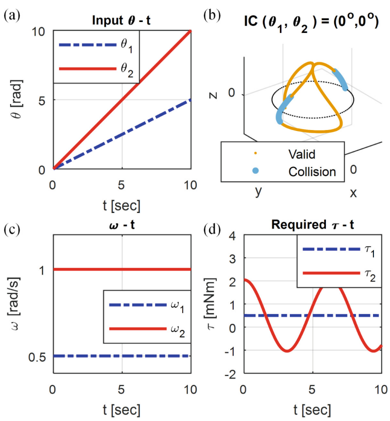

Fig. 6. Response of the mechanism running at constant ω using position control

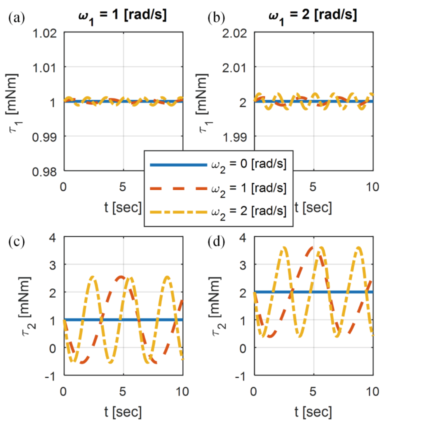

Fig. 7. Response of the mechanism running at different ω_1 and ω_2 conditions, with B_i are set 1 mNm · s/rad.

To find whether two links interact with one another, different step trajectories are selected as inputs, and the changes in torque response are observed. Noted that these trajectories are selected to be non-collision that are feasible during real applications. In Fig. 7(a) and (c), both actuators are set to be driven at same ω_1, and the values of ω_2 are adjusted. The results show that τ_1 remains nearly unchanged under different θ_2 input trajectories, and τ_2 appears to oscillate with the posture of Link 2. This corresponds to the observation from the governing equation that the gravity term is comparably larger than the others terms. Note that τ_2 is also combined with the centrifugal term, so increasing ω_1 will increase τ_2. This can also be proven with the simulation under different ω_1 settings, as shown in Fig. 7(b) and (d).

More trajectories were tested, including sine and polynomial input, during the trials. Since the mass and the centrifugal and Coriolis terms are small compared to the gravity term, the torque that arose from the motion effect would not have evident influence under the low ω area. Thus, when selecting actuators for the mechanism, τ_2 should be large enough to trigger the motion of Link 2, while τ_1 can be reduced to minimize the weight of the whole structure.

Moreover, to simulate the motion of the mechanism under force input, it is necessary to solve the dynamic equation for acceleration. We apply numerical integration techniques to integrate the acceleration and compute the future positions and velocities under the joint frame with the following equation:

$$\ddot{\Theta} = M^{-1}(\Theta)\left[\tau - V\left(\Theta, \dot{\Theta}\right) - G(\Theta) - F\left(\Theta, \dot{\Theta}\right)\right] \tag{6}$$

By solving the equation, we can predict the motion of the links under certain torque inputs, which means we can estimate the behaviors of the system under force control. Here, different step commands are selected as inputs to see the motion response of the model. The results show that the influences of θ_1 under different τ_2 inputs are nearly neglectable, while different input τ_1 could possibly affect the trajectories of both Link 1 and Link 2. However, using force control could not guarantee the posture of the both links, which may lead to collisions on the real mechanism. Therefore, position control is utilized to ensure non-interference between the links during practical applications.

To conclude this section, the simulation visualizes the dynamic response of the mechanism under position and force control. It provides advice on selecting the appropriate actuators. In addition, the simulation results show that the motion of Link 1 could possibly affect the behavior of Link 2, so compensating terms based on the equation of motion could be added into the command to increase the performance of the system when applying different control strategies.

5 Experimental Validation of the 2-DOF Mechanism

The prototype, as shown in Fig. 2(b), was built based on the morphology design described in Sect. 2 and the mechanism design reported in Sect. 3. The proposed 2-DOF mechanism was experimentally evaluated. To aid visualization, an LED was mounted on the end effector. The motion of the mechanism was recorded for a period of time (i.e. 15 s) while the LED was on Linkage L_2 (Fig. 2b). The trajectory of the end effector can be observed in the captured image. The results are shown in Figs. 8 and 9. The mechanism is placed vertically, with motor-1 located at the bottom to act as the base that connects the mechanism to the ground. The camera faced the top of the mechanism. In this first stage, the motors were driven using voltage control.

(a) Circular motion (b) Random motion

Fig. 8. The end effector trajectory where the first DOF performs continuous rotation.

The experiments included two parts, each demonstrating the continuous rotation of an individual DOF. In the first test, as shown in Fig. 8(a), the end effector started at the position shown by the red marker, while the second DOF (θ_2) was initially fixed at the edge of cylinder. After the first DOF (θ_1) rotated closed to a full circle, the second DOF raised the end effector to another orientation and then stopped. Then the first DOF continuously rotated for several circles. Figure 8(b) shows a scenario where the first DOF was driven continuously while the second DOF was moved randomly.

Figure 9 demonstrates the continuous rotation of the second DOF. In the experiment shown in Fig. 9(a), the end effector started from the center position, and then the second DOF was driven to rotate continuously while the first DOF was intermittently moved from a constant step to another step. In the experiment shown in Fig. 9(b), the first DOF was driven randomly.

(a) Circular motion (b) Random motion

Fig. 9. The end effector trajectory where the second DOF performs continuous rotation

In short, the experimental results confirm the feasibility of continuous rotation in both DOFs of the proposed 2-DOF mechanism. In other words, the use of two

C-shaped racks to connect two half-cylinders and avoid collision between the end effector linkage and the cylinder while maintaining the cylinder structure proves to be feasible and functional.

6 Conclusion and Future Works

We report on the development of an innovative 2-DOF mechanism that is capable of performing continuous rotation in both DOFs. The design process began with an analysis and comparison of general 2-DOF mechanisms, which were categorized as DD, DS, SD, and SS according to the arrangement of the transmission between motor-1 and the output axis as well as the output linkage to the end effector. The analysis revealed that only the SS type is capable of generating continuous rotation in both DOFs. Aiming to enlarge the range of continuous rotation in both DOFs, this work proposed a new type (SSD), which doubles the range of type SS. The design was realized as a detailed mechanism that is suitable for manufacturing, where the use of double C-shaped racks plays an important role owing to their functionality regarding both linkage avoidance and structure support. The dynamics of the 2-DOF mechanism were analyzed. The results reveal that the gravity effect plays a key role in the dynamics of the mechanism and that the two DOFs have a couple effect, whereby the first DOF affects the dynamics of the second DOF. A prototype was built and its performance was empirically evaluated in two sets of tests, where each test focuses on generating continuous rotation in one DOF while the other is fixed, moved in small steps, or moved randomly. The experimental results confirm the functionality of the continuous rotation of the two DOFs in the mechanism.

We are currently working on embedding electronic systems within the mechanism as well as using a feedback control strategy to quantitatively analyze the performance of the systems. We will then develop a suitable motion generation strategy to create a useful joint mechanism. In the meantime, we are also exploring the possibility of shrinking the size of the mechanism so that it can be utilized in applications with size constraints.

Acknowledgment. This work is supported by the Ministry of Science and Technology (MOST), Taiwan, under contracts MOST 108-2634-F-002-002.

References

1. Bajaj, N.M., Spiers, A.J., Dollar, A.M.: State of the art in artificial wrists: a review of prosthetic and robotic wrist design. IEEE Trans. Rob. **35**(1), 261–277 (2019)
2. Yu, O., et al.: Development of a new humanoid robot WABIAN-2. In: Proceedings 2006 IEEE International Conference on Robotics and Automation, 2006. ICRA 2006, pp. 76–81. IEEE, Orlando (2006)
3. Albers, A., et al.: Upper body of a new humanoid robot - the design of ARMAR III. In: 2006 6th IEEE-RAS International Conference on Humanoid Robots, pp. 308–313. IEEE, Genova (2006)

4. Gouaillier, D., et al.: Mechatronic design of NAO humanoid. In: 2009 IEEE International Conference on Robotics and Automation, pp. 769–774. IEEE, Kobe (2009)
5. Ott, C., et al.: Development of a biped robot with torque controlled joints. In: 2010 10th IEEE-RAS International Conference on Humanoid Robots, pp. 167–173. IEEE, Nashville (2010)
6. Lohmeier, S., Buschmann, T., Ulbrich, H.: Humanoid robot LOLA. In: 2009 IEEE International Conference on Robotics and Automation, pp. 775–780. IEEE, Kobe (2009)
7. Albers, A., Sander, C., Simsek, A.: Development of the actuation of a new wrist for the next generation of the humanoid Robot ARMAR. In: 2010 10th IEEE-RAS International Conference on Humanoid Robots, pp. 677–682. IEEE, Nashville (2010)
8. Nazri Bajuri, M., Abdul Kadir, M.R.: Computational Biomechanics of the Wrist Joint. Springer, Heidelberg (2013)
9. Kaneko, K., et al.: Humanoid robot HRP-3. In: 2008 IEEE/RSJ International Conference on Intelligent Robots and Systems, pp. 2471–2478. IEEE, Nice (2008)
10. Asfour, T., et al.: ARMAR-4: A 63 DOF torque controlled humanoid robot. In: 2013 13th IEEE-RAS International Conference on Humanoid Robots (Humanoids), pp. 390–396. IEEE, Atlanta, GA (2013)
11. Abdul Kadir, M.R.: Computational Biomechanics of the Hip Joint. Springer, Berlin, Heidelberg (2014)
12. Craig, J.J.: Introduction to Robotics: Mechanics and Control, 3rd edn. Pearson/Prentice Hall, Upper Saddle River (2005)